3D mapping of forced convection efficiency in reflow ovens

Balázs Illés / *Gábor* Harsányi

Abstract

In this paper, the investigation of the heating efficiency in forced convection reflow ovens which apply nozzle-matrix blower system is discussed. In these ovens the forced convection heat transfer coefficient (α) determines manly the efficiency of heating. Therefore we present here a method where the 3D distribution of α is determined from temperature distribution measurements in each heater zone of the reflow oven. The method has two steps: first, the temperature distribution in the oven is measured as a function of distance from the circuit board under chosen reference nozzle-line; in the second step, the heating efficiency of the neighbouring nozzle-lines is compared - at a dedicated measuring height - to the reference nozzle-line. From these data the distribution of α is calculated by the heat equation of the measurement system and extrapolated to the whole oven. The result is a 3D distribution map of α which is very important to the effective thermal modelling of the reflow soldering process and to the calibration of the reflow oven.

Keywords

forced convection · reflow oven · soldering

Balázs Illés

Department of Electronics Technology, BME, H-1111 Budapest Goldmann Gy. t. 3., building V2, Hungary
e-mail: billes@ett.bme.hu

Gábor Harsányi

Department of Electronics Technology, BME, H-1111 Budapest Goldmann Gy. t. 3., building V2, Hungary

1 Introduction

Nowadays, the reflow soldering process is the most widely used soldering technology in the electronics industry. The homogeneity and the efficiency of the heat transport have strong influence on the temperature profile of the reflow ovens. The inhomogeneous temperature profile causes reflow soldering failures.

The first reflow models dealt with the infra radiation (IR) ovens [10, 14, 15]. These were based on simplified expressions of heat radiation and conduction, and used only 2 dimensions. The mapping of IR ovens' capability started with simple temperature distribution measurements. These types of measurement systems had low resolution and accuracy [9, 14], therefore these are dated. The models in the "next generation" examined the reflow ovens which applied mixed heating (radiation & convection) [1, 11, 12]. These were still 2D, and sometimes applied the expression of convection heat transfer with wrong derivations (see in [1]). Actually, the latest reflow ovens use pure forced convection heating.

In this type of heater system, the efficiency is described by the forced convection heat transfer coefficient (α), [W/m²K]. Generally in a convection heat transport process the convection heat flow rate is calculated:

$$F_c(t) = \alpha \cdot S \cdot [T_2(t) - T_1(t)] \quad [\text{W}] \qquad (1)$$

where, S is the heated surface [m²] and $T_2(t) - T_1(t)$ is the temperature difference [K] between the heater gas and the heated surface. The convection heat is calculated by the integration of (1) over the time of the heating.

Useful simulations and numerical analysis of the forced convection [7, 8, 17] exist but not for reflow soldering environment. Although, a method for optimizing the heating capability of forced convection reflow ovens was published in [16], but it was based on a wrong correlation between α and the heater temperature. Several newer thermal models of the reflow soldering process [6, 13] still use an average or some different values of α for the whole oven, but this is a wrong approach. The value of α highly depends on the location in each heater zones. This is caused by the changes of the gas flow parameters, the inhomo-
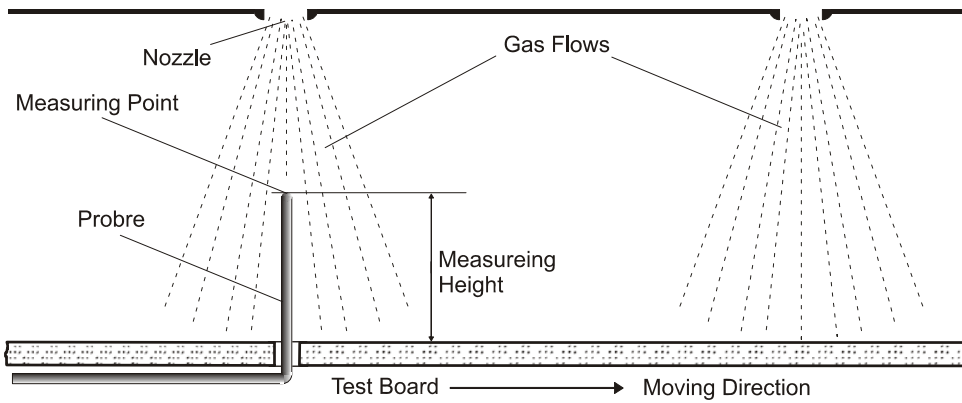
Fig. 1. Measuring position (cross section view)

geneity of the gas circulation system and the different contamination level of the blower system. Therefore the distribution of α in the reflow oven gives us valuable information about the capability of the oven.

There are two different methods to determinate α, these are the measurement or the calculation. Well worked out measurement method for the natural convection heat transfer has been published recently [2, 3]. The values of α in reflow ovens can be calculated using the following expression which has been derived from systematic series of experiments:

$$\alpha = \frac{\lambda}{2 \cdot d} \cdot G\left(g, \frac{H}{d}\right) \cdot Re^{\frac{2}{3}} \cdot \left[1 + \left(\frac{H/d}{0.6/\sqrt{g}}\right)^6\right]^{-0.05} \cdot Pr^{0.42} \quad (2)$$

where G and g are assistant functions depending on the geometry of the oven, λ is the thermal conductivity of the gas, Re is the Reynolds number and Pr is the Prandtl number of the gas [6]. But it is difficult to determine some parameters (e.g. the gas flow rate and density) which are needed for Re and Pr numbers.

Therefore we have developed a measurement method of forced convection efficiency in reflow ovens. The measurements were done in a pure forced convection reflow oven having 8 zones (7 heater zones). The investigated reflow oven applies the nozzle-matrix blower system. The nozzle-matrix is built up from parallel nozzle-lines which are also parallel with the moving direction of the assembly. These generate numerous blowing in heater gas flows. The assembled PCB passes under the nozzle-matrices during the soldering. Therefore the efficiency of the nozzle-lines can be studied.

2 Experimental analysis

Primary factors affecting the α are the gas flow parameters: flow rate, density and pressure of the heater gas. The exact measurement of these parameters is too complicated because of the extreme circumstances in the reflow oven (small space, high temperature, etc). Our alternative solution is the examination of the heating capability of the oven. We measure temperature changes and α is then calculated from the heat equation of the investigated reflow oven:

$$Q_a = Q_c + Q_k^* \quad (3)$$

where Q_a is the absorbed thermal energy during the soldering, Q_c is the convection heat and Q_k^* is the conduction heat. According to the construction of the forced convection reflow ovens we neglect the radiation heat.

2.1 Properties of the Measurement System

Point probes are required for the measurements in order to cause minimal disturbance of the gas flows. We applied K-Type rigid (steel coat) thermocouples pinned trough the prepared holes of the FR4 test board (Fig. 1). The measurements were done below the nozzle-lines facing to the blowing in gas flows. This position of the probes characterize most particularly the heating capability of the gas flow since we measure in the middle of them. The probes are parallel with the main flow direction and generate only one obstruction point in the gas flows. This obstruction point overlaps the measuring point. The disturbance of the gas flows is minimal therefore the measurement system is accurate for convection measurements.

The test board is 175 mm wide (this is a common size in the electronics industry), and does not contain any inner layer or any metallization on the surface, so its conduction behavior did not affect the measurement. The diameter of the thermo couples are only 1 mm. The rigid coat ensures that they hold their exact position during the measurements. The thermo couples are well insulated from the steel coat decreasing the conduction impact from the environment. But we should take into account the parasite conduction resistance R^* between the data recorder (DR) and the Measuring Point (MP). The conduction model of our measuring system is in Fig. 2.
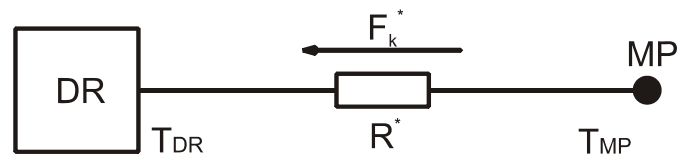

Fig. 2. Conduction model of the measuring system (illustration only for one probe)

The MP is modeled as a sphere and its conduction behavior is neglected because of the small dimensions. The thermal poten-

tial difference between the DR and MP ($T_{DR} - T_{MP}$) generates the parasite conduction heat flow F_k^* on R^*. Unfortunately the exact values of R^* and T_{DR} are unknown and F_k^* is not calculable. Therefore we used an offset calibration of the system (later in details) to eliminate the impact of F_k^*. The materials of the thermo couple are NiCr(90:10) – NiAl(95:5). These materials are well known, so the physical properties of the MPs can be exactly calculated (see Table 1).

Tab. 1. The physical properties of the MP

| Property	Value
Equivalent density, ρ [kg/m^3]	8.21×10^3
Equivalent thermal capacity, C [J/kgK]	4.74×10^2
Diameter, r_{MP} [m]	0.40×10^{-3}
Effective surface, $A = 4/3 \cdot \pi \cdot r_{MP}^2$ [m^2]	1.04×10^{-6}
Volume, $V = 4/6 \cdot \pi \cdot r_{MP}^3$ [m^3]	1.31×10^{-10}
Mass, $m = \rho \cdot V$ [kg]	1.07×10^{-6}

As we have mentioned, the nozzle-matrix is built up from parallel nozzle-lines. 12 nozzle-lines of the oven are located above the test board during the measurements. The common height of the SMD components are between 1-15 mm. In our investigation, we divided this range into 6 parts: 1, 3, 6, 9, 12 and 15 mm. To achieve the complete 3D α map of the oven using a 6 channel data register (6 pc. mes. height $\times$ 12 pc. n. line)/6 pc. data chanel $= 12$ measurement and $6 \times 12 = 72$ evaluation steps are needed. We simplified the method with the following considerations.

First, the temperature was measured under a chosen reference nozzle-line as a function of the distance from the board in each heater zones (1 measurement and 6 evaluation steps). Second, the temperature was measured under the 12 neighboring nozzle-lines at a dedicated distance from the board in each heater zones (2 measurements and 12 evaluation steps). The calculated α values of the reference nozzle-line can be extrapolated to the other nozzle-lines using the results of the second phase. Hence we get the 3D α map with only 3 measurements and 18 evaluation steps.

In the first phase, the nozzle-line NL 6 was chosen to reference line and the measurements executed below it in the distances of 1, 3, 6, 9, 12 and 15 mm from the test board (Fig. 4).

Six probes were applied and sent below all nozzles of the reference nozzle-line (like during the soldering). Hence the same nozzle-line in each heater zones was measured.

In the second phase, we have measured the temperature under the 12 neighboring nozzle-lines in each heater zones. The measuring height was 25 mm from the test board. This is the maximum height where we can measure due to the entrance gate of the oven. It is close enough to the entrance points of the gas flows; therefore this height is suitable for the comparison of the heating efficiency. The nozzle-line position above the board and the layout of the measurement system can be seen in the Fig. 5.
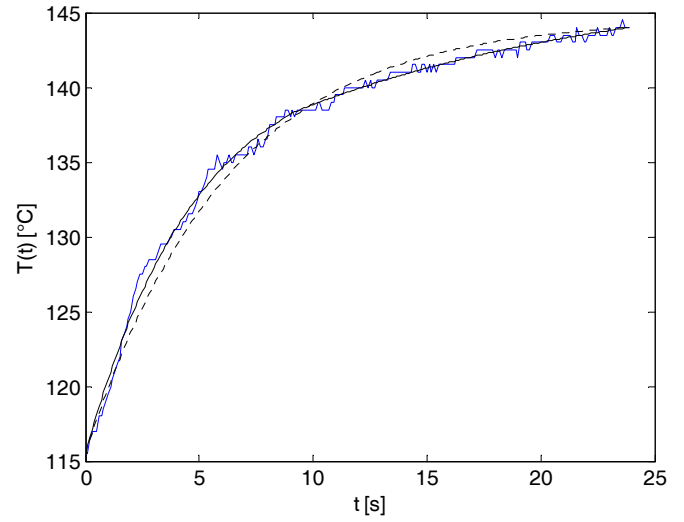
Fig. 3. Analytical curve fitting.

2.2 Data Processing and Calculation

A "Datapacq" type data recorder was used for the measurements. It was set to 0.1 s sampling time. The data were processed with "Reflow Tracker" and "Matlab 7.0" programs. As we expected the measured curves (the temperature changes) show exponential saturation (Fig. 6).

We have to fit analytical curves to the measured curves for the calculation of α. The temperature changes is modeled with exponential saturation:

$$T(t) = (T_h - T(t_0)) \cdot (1 - e^{-t/\tau}) \tag{4}$$

where T_h is the heater temperature, $T(t_0)$ is the initial temperature of the probe, t is the time and τ is the time coefficient of the heating:

$$\tau = t / \ln\left(1 - (T(t_r) - T(t_0))/(T_h - T(t_0))\right) \tag{5}$$

where $T(t_r)$ is the maximum temperature reached at the end of the heating.

The measuring device (just like the assemblies) has a cooling effect on the heater zones. This effect depends on the time and the location of the measuring device in the oven, because the oven tries to hold the set temperatures. Therefore, the exact T_h values of the measured curves should be calculated. This is carried out by an iteration curve fitting method. The T_h is iterated from the value of $T(t_r)$ using a 0.01°C temperature step up. In each iteration step, the model curves are fitted onto the measured curve. The iteration stops when the fitting failure reaches the minimal value.

In Fig. 3, the dashed line curve is calculated with only one T_h value (one fitting curve) for the whole curve. But T_h is changing during the measurement. If we apply two T_h values (two fitting curves) - one for the first part [t_0, t_1] and one for the second part [t_1, t_r] of the curve - the matching is much better (continuous line).

According to the foregoing Eq. (4) should be modified:

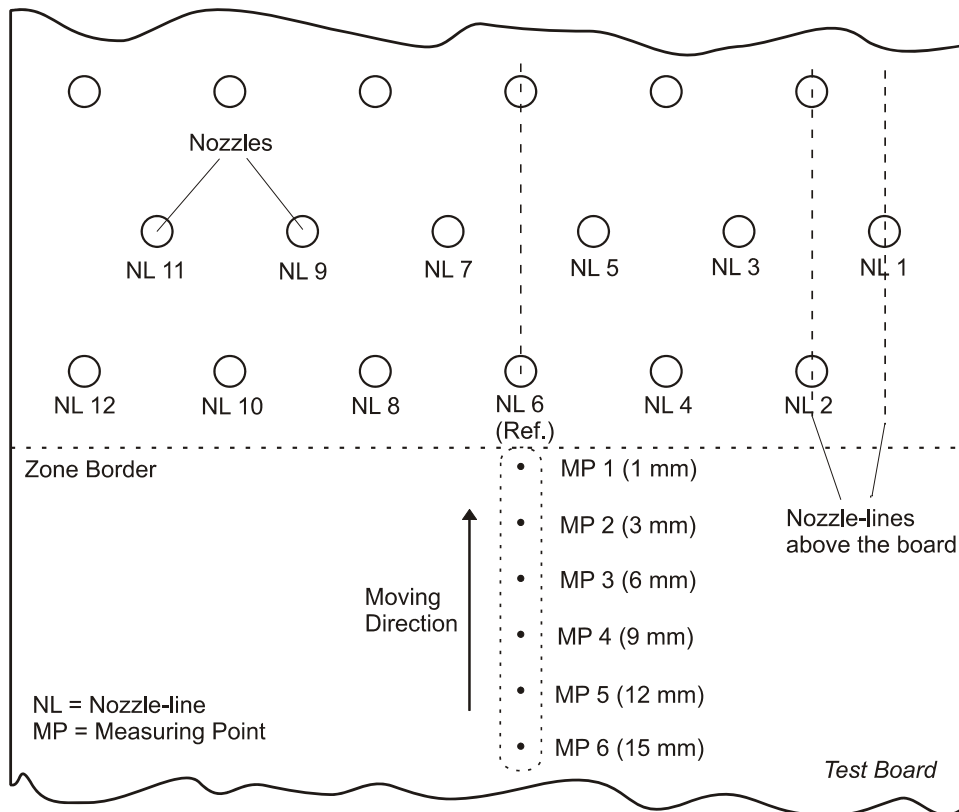$$T(t) = (T_h(t) - T(t_0)) \cdot (1 - e^{-t/\tau(t)}) \tag{6}$$

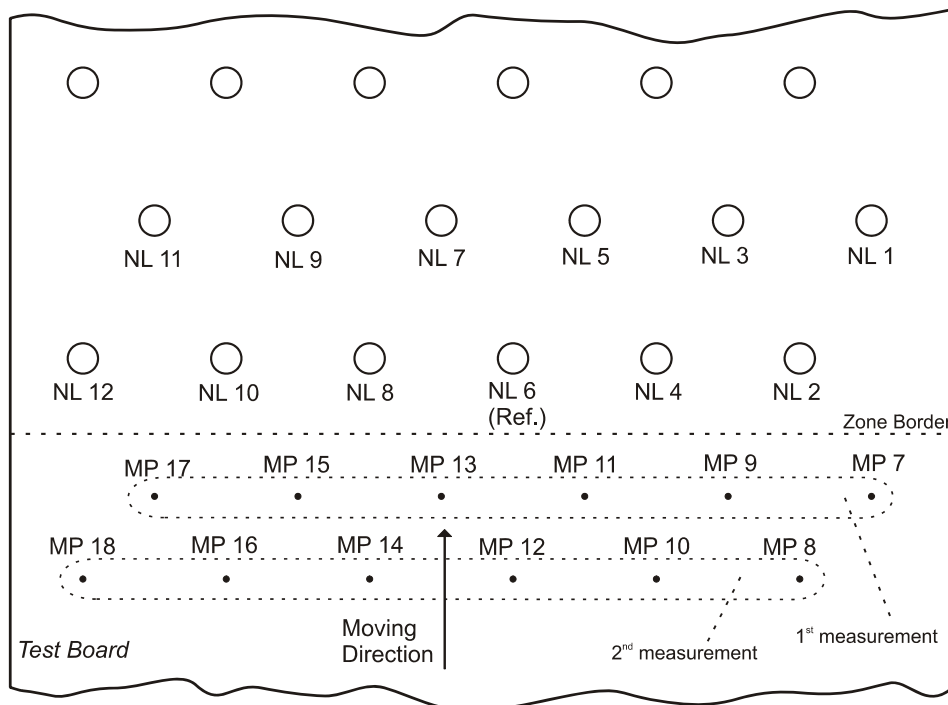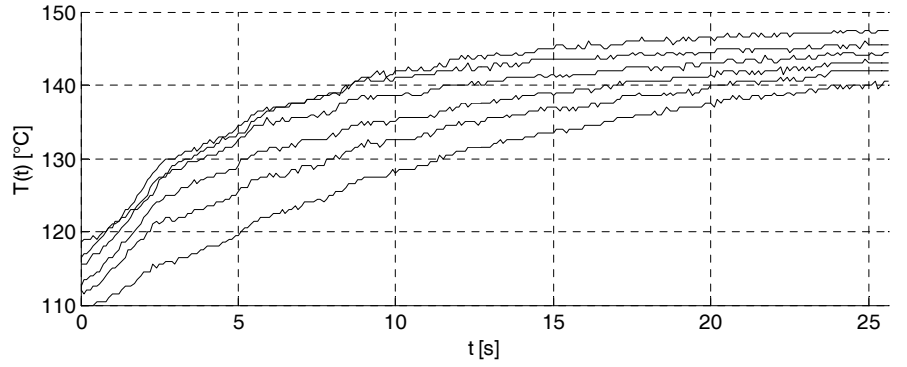**Fig. 4.** Measuring layout 1 (phase 1, top-view).

Fig. 5. Measuring layout 2 (phase 2, top-view).

Fig. 6. Measured curves in the 2nd (pre-heater) zone of the oven.

where $T_h(t) = \begin{bmatrix} T_{h1}|_{0-t_1} \\ T_{h2}|_{t_1-t_r} \end{bmatrix}$, and two time coefficient $\tau(t) = \begin{bmatrix} \tau_1|_{0-t_1} \\ \tau_2|_{t_1-t_r} \end{bmatrix}$ is needed.

The inner convection heat is calculated with the integration of (1) to the time interval of the heating $[t_0, t_r]$:

$$Q_c = \int_{t_0}^{t_r} F_c(t)\, dt = \int_{t_0}^{t_r} \alpha \cdot S \cdot (T_h(t) - T(t)) =$$
$$= \alpha \cdot S \cdot \big[(T_{h1} - T(t_0)) \cdot \tau_1 \cdot \big(1 - e^{-t_1/\tau_1}\big) \qquad (7)$$
$$+ (T_{h2} - T(t_1))) \cdot \tau_2 \cdot \big(1 - e^{-t_r/\tau_2}\big)\big]$$

Although the absolute measurement inaccuracy of the MP is $\pm 0.5°$C, but the expected value of the measurement failure is converging to zero due to the integration in Eq. (7). The amount of absorbed thermal energy is calculated:

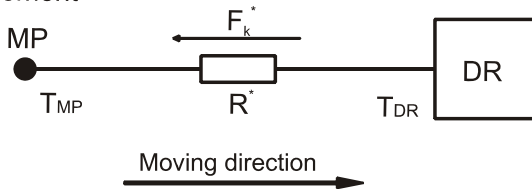$$Q_a = C \cdot m \cdot (T(t_r) - T(t_0)) \qquad (8)$$

where C is the thermal capacity and m is the mass of the measuring point.

As we mentioned above we eliminated the impact of parasite conduction F_k^* using a so called offset calibration. Two different arrangements for the measurement system should be used (Fig. 7).

1st arrangement
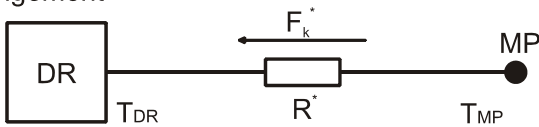
2nd arrangement

Fig. 7. Offset calibration of the measuring system.

In the first case the DR is positioned after the MP. This results in that $T_{MP} > T_{DR}$ and F_k^* has negative value in the heat equation (2). In the second (reverse) case the F_k^* has positive value in (2). Therefore, the addition of the heat equations of the two

different cases eliminates the effect of F_k^*. We defined a correction number in order to avoid the execution of this method for all measuring points. We compared 2×20 measurement results of the different arrangements and got the conclusion: α values of the first arrangement are about 9-11% larger than α values from the second arrangement. Consequently, we can eliminate the effect of F_k^* with a correction number ($k = 0.95$), applying it to the results of the first arrangement. α is calculated according to Eq. (2), (6) and (7):

$$\alpha = \frac{k \cdot Q_a}{\int_{t_0}^{t_r} S \cdot (T_h(t) - T(t))} [\text{W/m}^2\text{K}] \qquad (9)$$

From the results of the first phase (Fig. 3), α parameters of the reference nozzle-line $\alpha^{ref}(h, z)$ is calculated by Eq. (9) as a function of the measuring height (h) and heater zone (z). From the results of the second phase (Fig. 4), the ratio of the heating efficiency of the nozzle-lines (n) and the reference nozzle-line is calculated as a function of the heater zone (z):

$$\eta(n, z) = \frac{\alpha^n_{(25\,\text{mm})}}{\alpha^{ref}_{(25\,\text{mm})}} \qquad (10)$$

where $\alpha^{ref}_{(25mm)}$ is the forced convection heat transfer coefficient of the reference nozzle-line and $\alpha^{ref}_{(25mm)}$ is the forced convection heat transfer coefficient of the nozzle-line n at 25 mm above the test board. The forced convection constants can be extrapolated to the whole oven using the results of $\eta(n,z)$ and $\alpha^{ref}(h, z)$:

$$\alpha(n, z, h) = \eta(n, z) \cdot \alpha^{ref}(h, z) \qquad (11)$$

This 3D $\alpha(n,z,h)$ matrix gives the 3D α map of our reflow oven.

3 Results and Discussion

During the measurements, we have applied a widely used soak thermal profile for leaded solders. The set temperatures of the heater zones can be seen in Table 2. We could not process the results of the 7th (2nd peak zone) zone, because the temperature changes in this zone were too small, only 1-2°C.

As we discussed, the set temperatures of the heater zones are not equal to the real heater temperatures. In our case, T_h is modeled with $T_h(t) = \begin{bmatrix} T_{h1}|_{0-t_1} \\ T_{h2}|_{t_1-t_r} \end{bmatrix}$, where $t_1 = 70$ s. We observed considerable changes of the T_h values ($T_{h2} - T_{h1}$) during

Tab. 2. The set temperatures in the heater zones.

Heater zone	Temperature [˚C]
1	120
2	150
3	150
4	160
5	180
6 (peak 1)	245
7 (peak 2)	235

the measurement of the reference nozzle-line. It can be seen in Fig. 8 as a function of the measuring height separately in each heater zone.
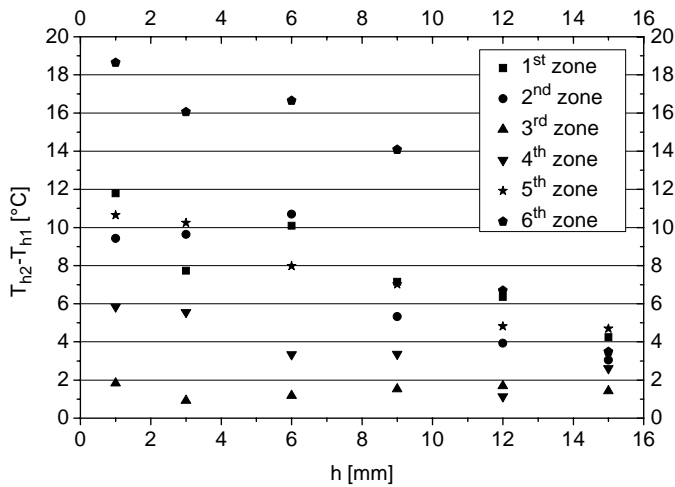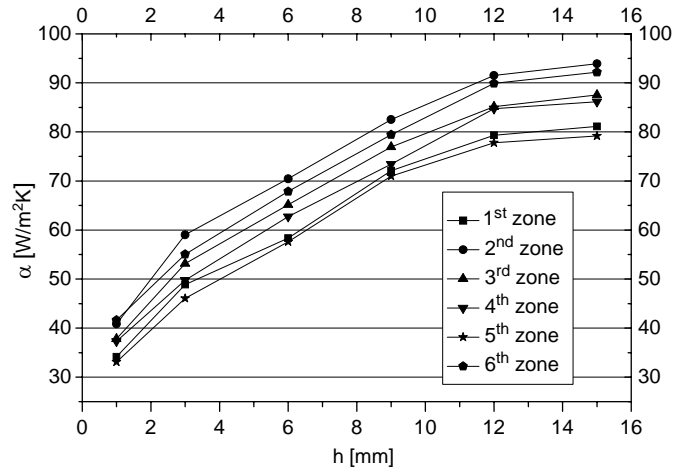

Fig. 8. $(T_{h2} - T_{h1})$ as a function of the measuring height.

As it was expected, we measured the highest changes of T_h (12-19˚C) in those heater zones where the gradient of the heating was also high (zone 1, 5 and 6). In all heater zones, bigger changes of T_h are located on lower measuring heights (1-3 mm), the changes of T_h are smaller on higher positions (on 15 mm it is only 2-5˚C).

The $\alpha^{ref}(h, z)$ results under the reference nozzle-line can be seen in Fig. 9 separately in each heater zones and measuring heights. The changes of α^{ref} values follow a similar shape in each heater zones of the oven. The curves have two breaking-points; α^{ref} is considered to be constant from the entrance point of the gas flows to 12 mm, from 12 mm to 3 mm the decline starts and follows a linear shape, at 3 mm there is a cut-off point and the gradient of the decline grows. As we expected before, the changes of α^{ref} values are very high as a function of the measuring height. These results prove our calculated results from previous studies about the gas flows in forced convection reflow ovens [4, 5]. Our former calculations have shown that α of the heater gas is near constant as a function of the height (blower phase) until a point where the gas flow direction begins changing (transition phase). This point is about 12 mm above the board according to our measurements. It should be also noted that the efficiency differences between the heater zones

are 15-20%.

Fig. 9. $\alpha^{ref}(h, z)$ values of the reference nozzle-line as a function of measuring height.

The result of the heating efficiency comparisons $\eta(n,z)$ can be seen in Fig. 10. The efficiency differences between the nozzle-lines are 20-40% in one zone. It is caused by different effects, for instance: the variation of the gas flow parameters, the inhomogeneities of the gas circulation system, the different contamination level of the gas blower system, etc.

The 3D α map is generated by Eq. (11) from the data of Fig. 9 and Fig. 10. The best way for visualization of the 3D α map is the separation of it into layers according to the measuring height. The values of the α map at 3 mm measuring height are visualized in Fig. 11 after a linear interpolation. This visualization method ensures that we get sufficient view about the changes of α in the oven.

Considerable heat transfer coefficient differences were observed in the different heater zones and nozzle-lines, the maximum difference was almost 85%. On the average the convection efficiency is higher in the middle of the board. This is probably caused by the gas flow circumstances above the board. These effects generate inhomogeneous thermal distribution in the oven.

4 Conclusions

In this paper, 3D mapping of the heat transfer coefficient (α) in a forced convection reflow oven is discussed. We measured that the assemblies cause high changes of the heater temperature (T_h) in the heater zones during the soldering (Fig. 8). In all heater zones, bigger changes of T_h (12-15˚C) are located on lower measuring heights, the changes of T_h are smaller on higher measuring points (on 15 mm it is only 2-5˚C). Our results showed that α highly depends on the distance from the board (Fig. 9.), which shows linear shape sections with different gradients. High efficiency differences were observed between the heater zones (15-20%) as well between their nozzle-lines (20-40%) and accumulated differences in α as high as 85%. These effects generate inhomogeneous α distribution in the reflow oven (Fig. 11). This can cause inhomogeneous thermal
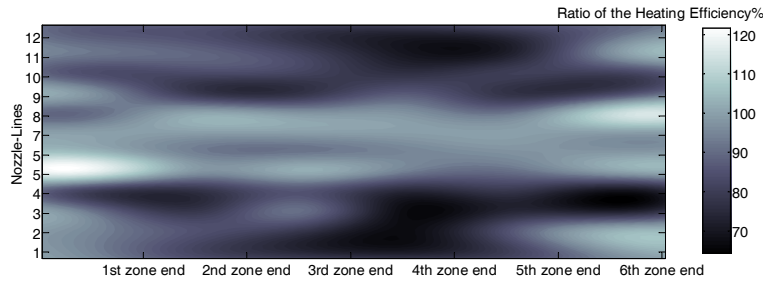
Fig. 10. Heating efficiency comparison $\eta(n,z)$ to the reference nozzle-line.
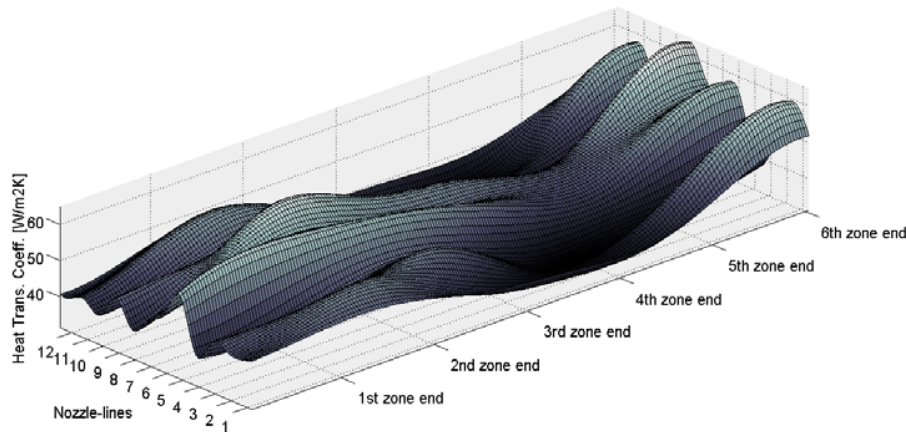

Fig. 11. α map of the reflow oven at 3 mm above the board.

profile which leads to soldering failures. But in the possession of the 3D α map of the reflow oven, effective thermal simulations, failure predictions, heating and layout optimization can be carried out. Therefore our monitoring system is a useful tool for electronics production. The measurement approach presented here is also applicable for optimizing other type of heater systems which apply forced convection heating.

References

1 **Carson J K, Willix J, North M F**, *Measurements of heat transfer coefficients within convection ovens*, Journal of Food Engeeniering **72** (2006), 293–301, DOI 10.1016/j.jfoodeng.2004.12.010.

2 **Evtatiev I, Pencheva T, Mashkov P**, *Heat Transfer Modeling for Soldering Processes of SMD's to Printed Circuit Boards Using Low Inert Infrared Heaters*, 28th Int. Spring Seminar on Elctronics Technology, 2005.

3 **Hanreich G, Nicolics J**, *Measuring the Natural Convective Heat Transfer Coefficient at the Surface of Electronic Components*, Instrumentation and Measurement Technology Conference, 2001.

4 **Illés B., Krammer O, Harsányi G, Illyefalvi-Vitéz Zs**, *Modelling Heat Transfer Efficiency in Forced Convection Reflow Ovens*, 29th Int. Spring Seminar on Elctronics Technology, 2006, pp. 80–85.

5 **Illés B., Krammer O, Harsányi G, Illyefalvi-Vitéz Zs, Szabó A**, *3D Thermodynamics Analysis Applied for Reflow Soldering Failure Prediction*, 4th European Microelectronics and Packaging Symposium, 2006, pp. 217–222.

6 **Inoue M, Koyanagawa T**, *Thermal Simulation for Predicting Substrate Temperature during Reflow Soldering Process*, Electronic Components and Technology Conference, 2005, pp. 1021–1026.

7 **Juncu G**, *A numerical study of momentum and forced convection heat transfer around two tandem circular cylinders at low Reynolds numbers. Part II Forced convection heat transfer*, Inernational Journal of Heat and Mass Transfer **50** (2007), 3799–3808, DOI 10.1016/j.ijheatmasstransfer.2007.02.021.

8 **Mistry H, Subbu G, Dey S, Bishnoi P, Castillo J L**, *Modeling of transient natural convection heat transfer in electric ovens*, Applied Thermal Engeeniering **26** (2006), 2448–2456, DOI 10.1016/j.applthermaleng.2006.02.007.

9 **Rosu B, Reyes-Turcu P., Simion-Zanescu D**, *Thermal management system for reflow oven*, 28th Int. Spring Seminar on Elctronics Technology, 2006, pp. 294-298.

10 **Sarvar F, Conway P P**, *Effective modelling of the reflow soldering process: basis construction and operation of a process model*, IEEE Trans. Components Packaging Manuf. Technol. Part C: Manuf., 1998, pp. 126–133.

11 **Simion-Zanescu D, Svasta P, Streza F**, *Self-Teaching Setup for Reflow Soldering Process*, 28th Int. Spring Seminar on Elctronics Technology, 2005, pp. 294–298.

12 **Simion-Zanescu D, Svasta P**, *Particularities of Reflow soldering model*, 11th Int. Symposium for Design and Technology of Electronic Packages, 2005, pp. 113–116.

13 **Steenberge N V, Limaye P, Willems G, Vandevelde B, Schildermans I**, *Analytical and finite element models of the thermal behavior for lead-free soldering processes in electronic assembly*, Microelectronics Reliability **47** (2007), 215–222.

14 **Whalley D C**, *A simplified reflow soldering process model*, Journal of Materials Processing Technology, 2004, pp. 134–144, DOI 10.1016/j.jmatprotec.2004.01.029.

15 **Wu C H, Srihari K, McLenaghan A J**, *A knowledge-based thermal profile identification advisor for surface mount PCB assembly*, The International Journal of Advanced Manufacturing Technology **11** (1996), 343–352, DOI 10.1007/BF01845693.

16 **Yamane M, Orita N, Miyazaki K, Zhou W**, *Development of New Model Reflow Oven for Lead-Free Soldering*, Furukawa Review **26** (2004), 31–36.

17 **Yin J, Wang B C, Bergstrom J D**, *Large-eddy simulation of combined forced and natural convection in a vertical plane channel*, International Journal of Heat and Mass Transfer, 2007, pp. 3848–3861, DOI 10.1016/j.ijheatmasstransfer.2007.02.014.